ISSN 0031-918X, The Physics of Metals and Metallography, 2015, Vol. 116, No. 6, pp. 576–585. © Pleiades Publishing, Ltd., 2015.
Original Russian Text © A.D. Pogrebnyak, Yu.A. Kravchenko, A.A. Dem'yanenko, O.V. Sobol', V.M. Beresnev, A.V. Pshik, 2015, published in Fizika Metallov i Metallovedenie, 2015, Vol. 116, No. 6, pp. 610–620.

STRUCTURE, PHASE TRANSFORMATIONS, AND DIFFUSION

Peculiarities of the Formation of Multicomponent $AlN–TiB_2–TiSi_2$ Composite Ceramics Coatings during Heat Treatment

A. D. Pogrebnyak[a], Yu. A. Kravchenko[a], A. A. Dem'yanenko[a], O. V. Sobol'[b], V. M. Beresnev[c], and A. V. Pshik[a]

[a]*Sumy State University, ul. Rimskogo-Korsakova 2, Sumy, 40000 Ukraine*
[b]*Khar'kov Technical University KhPI, ul. Frunze 21, Khar'kov, 61000 Ukraine*
[c]*Khar'kov National University, pl. Svobody 4, Khar'kov, 61077 Ukraine*
e-mail: alexp@i.ua

Received August 13, 2014; in final form, October 14, 2014

Abstract—Results of studies of the morphology, elemental and phase compositions of coatings prepared by pulsed magnetron sputtering of the $AlN–TiB_2–TiSi_2$ composite ceramic target have been reported. The used technology allows us to prepare a protective amorphous-like layer with ordering areas with sizes up to 1 nm. The heat treatment of samples at 900 and 1300°C leads to the depletion of the coating surface of boride phases and the formation of α-Al_2O_3- and β]-TiO_2-based protective films on the surface. The growth of crystallites of the nanostructured coating to 11–25 nm is observed. The annealing at 1300°C allows us to obtain the thermally stable crystalline state of substance, the nanohardness of which is 11 GPa.

Keywords: nanocomposite coating, pulsed magnetron sputtering, high temperature annealing, phase and elemental composition, amorphous-like structure, nanohardness

DOI: 10.1134/S0031918X15040122

INTRODUCTION

The increasing demands of process efficiency (machining rate) and quality of machine components in combination with established ecological standards lead to systematically increasing requirements for the physical and mechanical properties of the surface of articles [1]. Moreover, there is a need to produce articles characterized by high hardness and oxidation stability. Traditional coatings based on transition-metal nitrides, in particular based on TiN, allow one to solve the problem of increasing the hardness [2, 3], surface wear resistance [4, 5], and corrosion resistance in aggressive media [3, 6]. However, the main disadvantage of the coatings is their limited oxidation stability at high temperatures [7]. The incorporation of Al and Si into the titanium nitride allows one to modify the surface protective properties. In particular, Al additions in TiN lead to the formation of $Ti_xAl_yN_z$ coatings characterized by the high hardness (≈32 GPa) [8] and oxidation stability (to 800°C) [9]; surface alloying with Si ions increases the abrasive (wear) resistance of surface and stability during sputtering with metal ions [9].

Nanocomposite TiSiN coatings are most understood. They consist of TiN nanocrystals embedded into an amorphous silicon nitride matrix. These coatings are characterized by high oxidation stability at temperatures close to 850°C and are superhard (>40 GPa) and thermally stable to 1100°C [10–12].

Recently, results of studies of four-component nanocomposite TiAlSiN coatings that consist of $Ti_{1-x}Al_xN$ crystalline and Si_3N_4 amorphous components have been obtained [13, 14].

The application of multicomponent and multilayer coatings (the layer thickness equals several nanometers) allows us to obtain protective layers characterized by high thermal stability of physical and mechanical properties and thermal oxidation stability [15]. The need for continuous operation of machinery is the cause of the formation of multilayer coatings based on multicomponent materials, such as TiN/SiN_x [16], $TiAlSiN/Si_3N_4$ [17], TiCrN/AlSiN [18], TiAlCrN/AlSiN [19], etc. It was shown in [16–19] that the properties of multilayer nanoscale coatings are determined mainly by the thickness, number of individual layers, diffusion and phase-formation processes in them as well. The use of TiAlN and TiAlSiN for the formation of multilayer coatings allows one to obtain the superhard surface that, due to the incorporation of plastic TiAlN layers, is resistant to deformation under external loading [20].

It should be noted also that, recently, the development of coatings containing five or more components is an actual problem. In the case of correctly selected

Table 1. Parameters of the deposition process and annealing of $AlN–TiB_2–TiSi_2$ coatings

Series no.	U_{pulsed}, V	I, A	U_{cm}, V	Annealing conditions (in air)
1	700	2	200	Initial state
2				Samples were heated to 200°C for 15 min, then to 900°C for 60 min, after which they were held at this temperature for ~60 min.
3				Samples were heated to 200°C for 15 min, then to 1300°C for 90 min, after which they were held at this temperature for ~60 min and subjected to uncontrollable cooling to 0°C.
4	To study the effect of ion implantation, samples of series 3 were subjected to bombardment with Au ions with an energy of 40 keV to an irradiation dose of 10^{17} cm^{-2}.			

U_{pulsed} is the pulsed voltage at the sputtered target and U_{bias} is the bias voltage at the substrate.

components of the material, a coating made of the material has significant advantages over coatings consisting of less number of components [21].

The aim of the present study is to perform complex investigations of the structure, phase composition, morphology of the surface, and the physical and mechanical characteristics of coatings prepared by the pulsed magnetron sputtering of $AlN–TiB_2–TiSi_2$ composite ceramics.

EXPERIMENTAL

Coatings were prepared by pulsed magnetron sputtering using a setup, the diagram of which is described in [22]; the coatings were deposited on steel-45 substrates. As the sputtered material, we used high-temperature composite $AlN–TiB_2$ systems with a $TiSi_2$ titanium silicide addition developed at the Frantsvich Institute for Problems of Materials Science, National Academy of Sciences of Ukraine. Since multicomponent multilayer coatings are characterized by low adhesion activity [15], we used polished substrates to qualitatively estimate the adhesion. Before the deposition of the coating, in order to ensure the pure crystalline interface (that accelerates the epitaxial growth of coating), the substrate surface was purified with respect to gas ions and oxide and carbide impurities, as well using a glow discharge (the argon pressure is 0.08 Pa and the treatment time is 15 min). The subsequent magnetron sputtering and deposition of material on the substrate was realized for 35 min at a partial argon pressure in the chamber of ~0.1 Pa. Table 1 shows the conditions of the deposition and subsequent treatment of samples.

The morphology and elemental composition of the surface were studied using a scanning electron microscope equipped with an attachment for the energy dispersive X-ray analysis (SEM/EDS) and an accelerating voltage of 20 kV. The coating thickness and state of the coating–substrate interface were determined using fractographs taken with a Quanta 600 FEG electron microscope. The surface profile and sizes of surface roughness were determined using a VK-X100/X200 scanning microscope equipped with a 3D laser.

To analyze the structural and phase states of samples, we used a DRON-3M diffractometer and Cu $K\alpha$ radiation. The phase composition was studied using traditional X-ray diffraction techniques, namely, the analysis of angular positions, intensities, and profiles of diffraction reflections. To interpret X-ray diffraction patterns, we used the Powder Diffraction File (International Center for Diffraction Data). Additional studies of the phase composition of the coatings were performed by small-angle scattering using Cr $K\alpha$ radiation. X-ray spectroscopy was performed using a RINT-2500 V diffractometer and a position-sensitive proportional counter (PSPC/MDGT).

The mechanical characteristics (hardness and modulus of elasticity) of the $AlN–TiB_2–TiSi_2$ coatings were determined by nanoindentation using a Hysitron TI 950 Triboindenter and a Berkovich trihedral indenter. In order to exclude the substrate effect on the experimental data on the hardness and modulus of elasticity, the indenter loading was chosen so that the depth of penetration does not exceed 10% of the coating thickness.

RESULTS AND DISCUSSION

Electron-microscopic studies of the surface topography of coatings based on the $AlN–TiB_2–TiSi_2$ composite ceramics (Fig. 1) showed that, under the used deposition conditions, the protective layer characterized by uniform structure with a negligible content of 1-μm-sized drops (up to 10 μm in diameter) is formed. A fairly flat surface is observed in areas free of these growth defects.

Figure 2a shows a micrograph that demonstrates the morphology of the $AlN–TiB_2–TiSi_2$ coating surface, which is taken with the 3D laser. Estimating the surface roughness has showed that the used deposition conditions allow us to form the coating with rough mircoedges less than 1 μm in size (Fig. 2b). This fact indicates the high quality of coating prepared by magnetron sputtering of a target that has the multicomponent composition.

We assume that the appearance of the inclusion on the coating surface is due to the local inhomogeneity

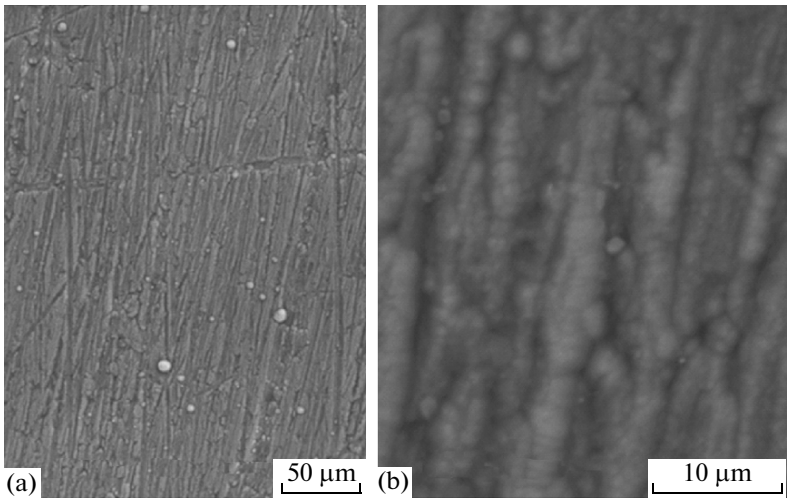

Fig. 1. Surface morphology of the AlN–TiB_2–$TiSi_2$ coatings (series 1) studies with magnifications of (a) 300× and (b) 2500×.

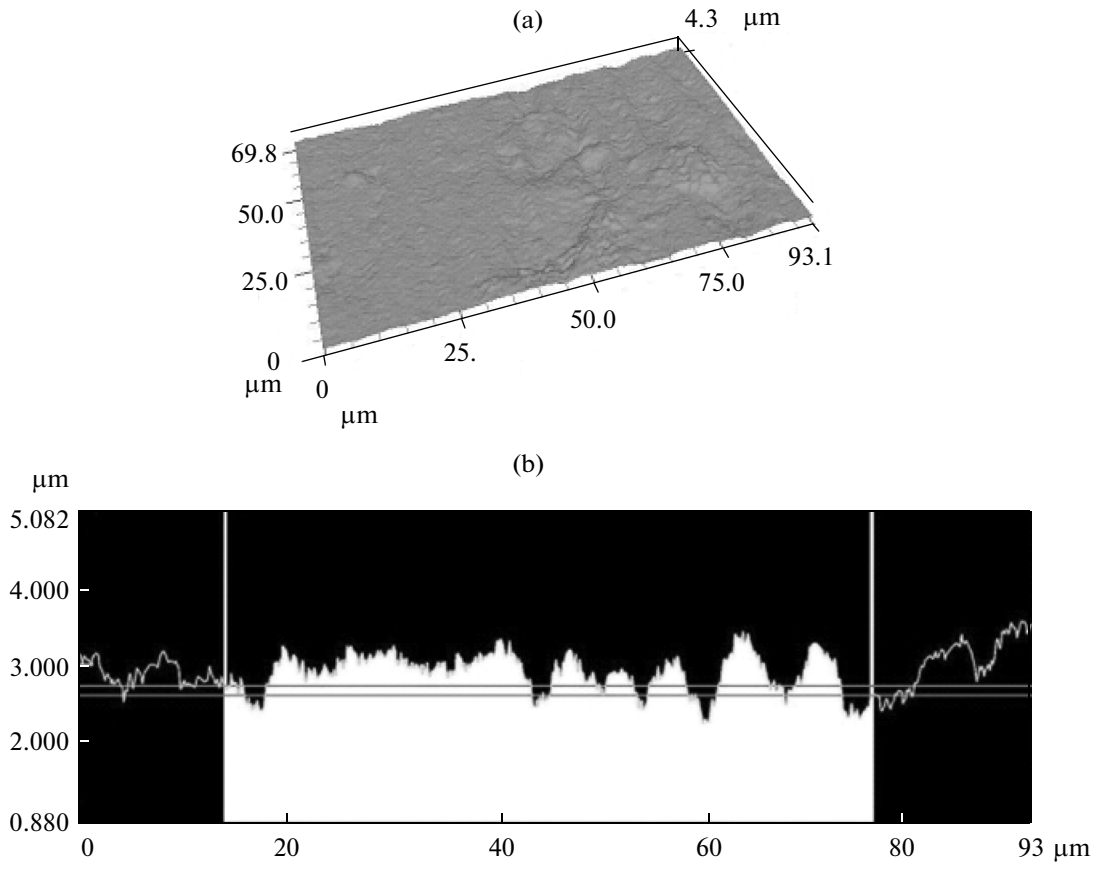

Profile	Horz. dist.	Hght. diff.	Hght. ave	Angle	C.S. length	C.S. area	R	Comment
All	93.00 μm	0.379 μm	2.911 μm	0.233°C	106.786 μm	200.418 μm^2		
Seg. 1	62.794 μm	0.130 μm	2.888 μm	0.119°C	72.940 μm	133.962 μm^2		

Fig. 2. (a) Surface local inhomogeneities of coating in the initial state and (b) distribution profile taken with 3D laser and optical methods.

Table 2. Elemental composition of $AlN–TiB_2–TiSi_2$ coatings

Series no	T_{an}, °C	Content of elements in the coatings, at %						
		B	C	O	N	Al	Si	Ti
1	–	34.49	17.27	11.92	9.26	17.25	2.89	6.92
2	900	38.07	12.70	13.14	8.32	18.30	2.70	6.72
3	1300	23.57	30.36	26.84	6.97	11.45	0.32	0.49

of its composition. Table 2 shows the integral elemental composition determined by X-ray spectroscopic analysis. According to these data, the matrix of starting coatings is based on metallic Al; among light elements, boron is the leading component. The great number of components in the coating composition makes it difficult to analyze diffusion processes during deposition and, therefore, to find the causes of the formation of local inhomogeneous areas on the surface. According to the data of X-ray spectroscopy, the composition of the inclusion comprises 38.71 at % B, 15.12 at % C, 15.87 at % N, 9.62 at % O, 10.75 at % Al, 1.55 at % Si, 4.36 at % Ti, and 4.01 at % Fe. The depth of electron penetration exceeds the size of the drop, which is why iron is present in the coating composition. In this case, the characteristic X-ray radiation from the steel substrate is recorded.

The phase composition of the $AlN–TiB_2–TiSi_2$ composite ceramics used for coating deposition includes phases with the melting temperatures above 1500°C. Therefore, the thermal annealing at 900°C gives no substantial changes in the surface morphology (Fig. 3). Micrographs taken with the 2500× magnification show that, as a result of annealing, surface inclusions with diameters of up to 0.5 μ disappear. Submicron-sized relief characterized by globular inclusions is formed against a background of micron-sized macrorelief. The inclusions can result from the formation of Ti- and Al-based oxide phases. The 2D images of the surface demonstrate its developed topology; it is obvious that the rough edges exceed 1 μm (Fig. 4).

The holding of samples at 1300°C activates recrystallization processes occurring in the material, and the coating is in part melted. The clear globular substructure is absent; at the microlevel, numerous various small inclusions appear (Fig. 5). It should be noted that they do not favor the formation of surface with the developed relief. Moreover, the high-temperature annealing leads to the marked decrease in the surface roughness of the protective layer (Figs. 2b, 4b, 6b).

The integral elemental composition of the surface is identical to the initial composition of coatings (Table 2). High-temperature annealing at 1300°C leads to the depletion of the coating of boron and oxygen; the titanium and silicon contents decrease to 0.5 at %. It is known that, in titanium compounds ($T_m(Ti_5Si_3)$ = 1330°C and $T_m(TiSi_2)$ = 1500°C), silicon forms a low-melting eutectic; a silicon addition to the $TiSi_2$ com-

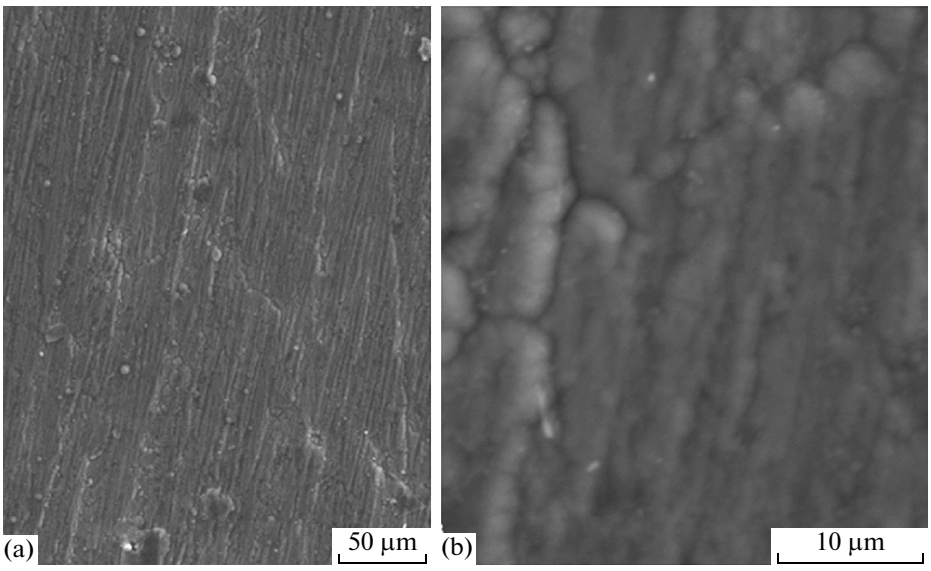

Fig. 3. Electron-microscopic images of the surface of coatings (series 2) annealed at 900°C taken with magnifications of (a) 300× and (b) 2500×.

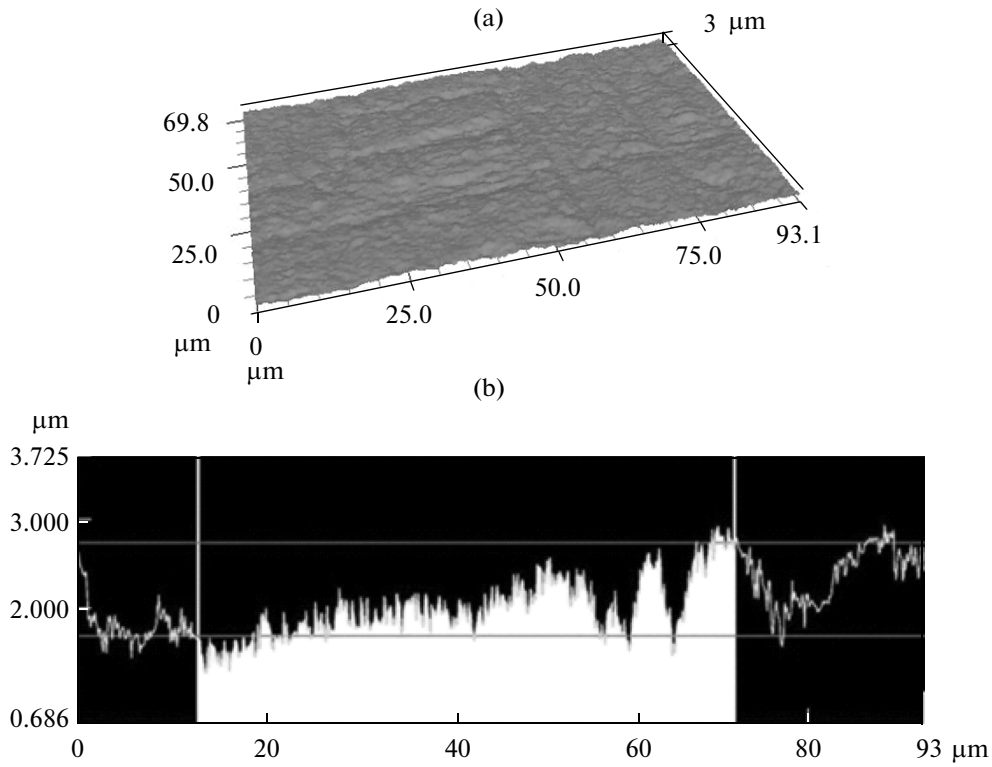

Profile	Horz. dist.	Hght. diff.	Hght. ave	Angle	C.S. length	C.S. area	R	Comment
All	93.000 μm	0.044 μm	2.061 μm	0.027°C	130.827 μm	128.042 μm^2		
Seg. 1	58.532 μm	1.044 μm	2.001 μm	1.022°C	83.098 μm	77.025 μm^2		

Fig. 4. Effect of high-temperature annealing at 1300°C on the (a) surface topology and (b) substance distribution profile.

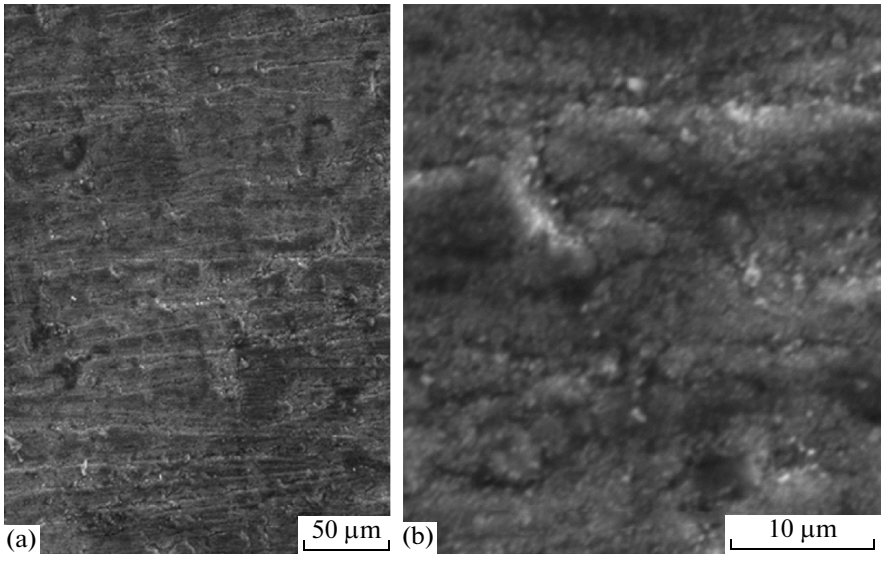

Fig. 5. Surface morphology of the AlN–TiB_2–$TiSi_2$ coatings (series 3) annealed at 1300°C.

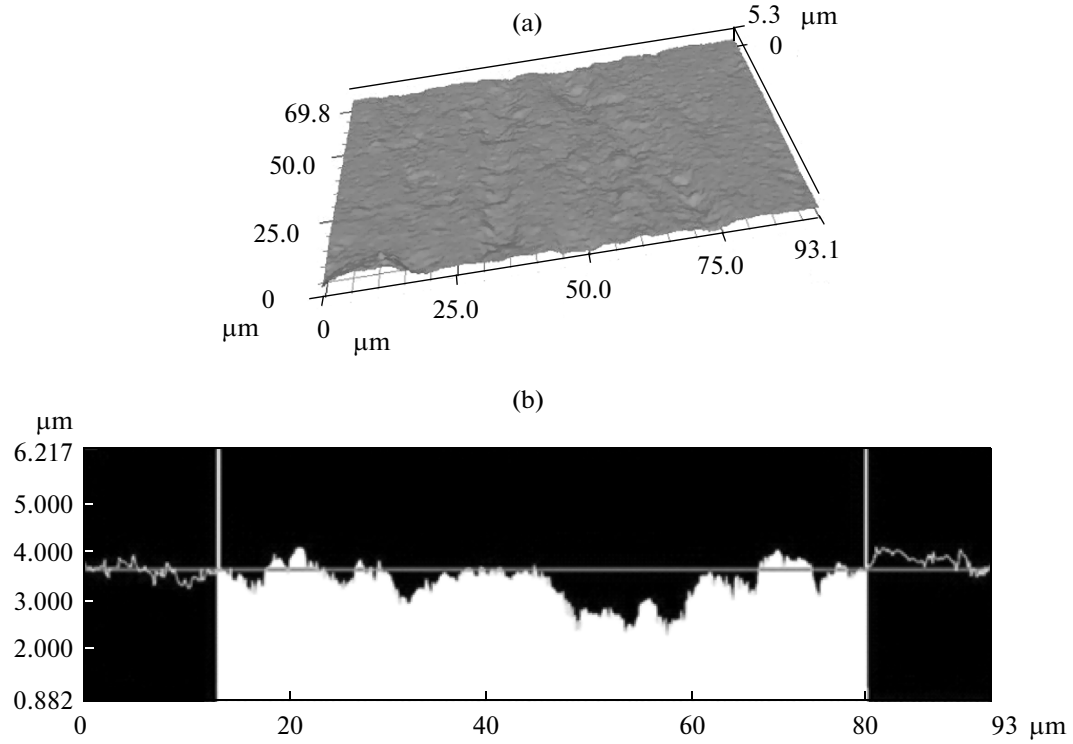

Profile	Horz. dist.	Hght. diff.	Hght. ave	Angle	C.S. length	C.S. area	R	Comment
All	93.000 μm	0.137 μm	3.497 μm	0.085°C	113.189 μm	243.407 μm^2		
Seg. 1	65.802 μm	0.054 μm	3.395 μm	0.047°C	80.603 μm	165.376 μm^2		

Fig. 6. (a) Surface local inhomogeneities of coating in the initial state and (b) distribution profile taken with 3D laser and optical methods.

pound substantially decreases its melting temperature. Because of this, despite that T_m(Ti) = 1668°C and T_m(Si) = 1414°C, we assume that the chemical composition of the surface is the cause of the evaporation of titanium and silicon at 1300°C.

According to the data of X-ray diffraction analysis (Fig. 7), a coating with an amorphous-like structure is formed during deposition. The X-ray diffraction pattern demonstrates a halo, the width and maximum of which correspond to $2\theta \sim 20°–25°$ and $2\theta \approx 40°$, respectively; no clear diffraction peaks are observed. However, the analysis of micrographs of fractures (Fig. 8) indicates the presence of crystalline structure in the protective coating. The results obtained agree with each other when we assume that the coatings consist of nanocrystalline particles. According to [23], this is quite possible since X-ray diffraction patterns of amorphous and nanocrystalline materials are similar and can be observed in the case of the amorphous (in terms of X-ray diffraction) state. Thus, the deposited coatings are characterized by the absence of long-range order in the substance structure; however, a short-range order is observed within several interparticle distances.

The sizes of areas in which the same physical magnitudes correlate to one another were estimated in accordance with the procedure described in [24]. In the calculations, it was taken into account that the correlation radius R_m is in inverse proportion with the

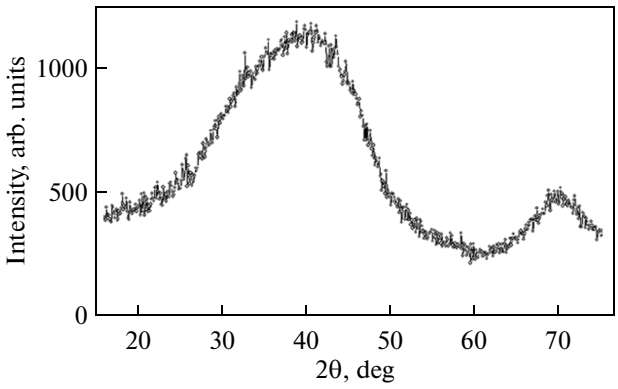

Fig. 7. Portion of X-ray diffraction pattern for theAlN–TiB_2–$TiSi_2$ coating prepared by pulsed magnetron sputtering.

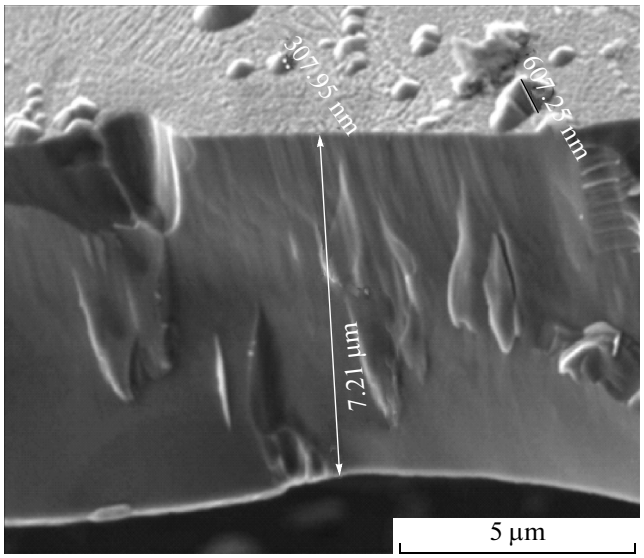

Fig. 8. Micrograph of the fracture pattern of the coating (series 1).

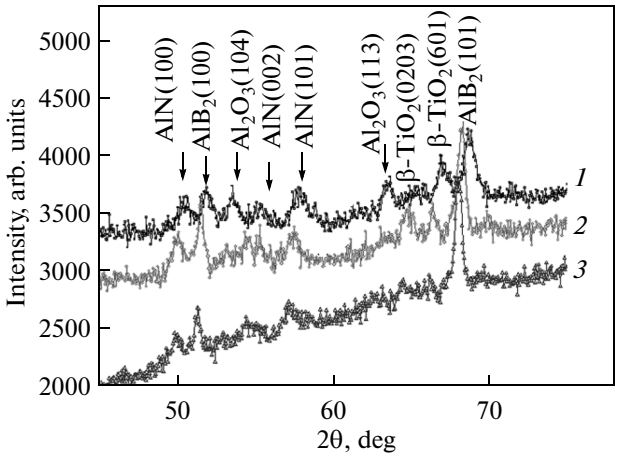

Fig. 9. Portions of X-ray diffraction patterns for the composite coating (series 2) annealed at 900°C taken at tilting angles of (*1*) 3°, (*2*) 10°, and (*3*) 30°.

width of the first wide-angle halo-like curve, Δs, which is plotted on intensity–scattering vector $\vec{s}$ coordinates as follows:

$$R_m = \frac{2\pi^3 z^2}{6.25\Delta s} \approx \frac{9.907}{\Delta s}, \quad (1)$$

where $z = 1$ is the index of the first maximum, $s = |\vec{s}| = 4\pi\frac{\sin\theta}{\lambda}$ is the modulus of scattering vector, θ is the half of scattering angle, and λ = 1.54178 Å is the wavelength of characteristic radiation.

Thus, during deposition, an amorphous-like coating is formed, which is characterized by ordering areas with sizes of about 1 nm (R_m).

The main task of the investigation is the formation of a protective multicomponent coating characterized by high physical and mechanical properties and chemical stability of the system at temperatures above 1000°C. One of the methods of obtaining a surface that exhibits high oxidation stability is to form a protective coating based of noncrystalline structures. It is known that this structure determines the absence of paths for easy diffusion and, therefore, the increase in the diffusion stability under external actions. However, these structures are metastable at high temperatures and, during heating in the course of operation, the protective layer undergoes softening.

The presence of a crystalline structure in the surface composition allows one to accelerate the diffusion of impurity atoms along grain boundaries toward the coating–substrate interface and to exclude the possibility that the material will oxidize over the volume of the protective layer. To increase the oxidation stability of crystalline coatings, paths for atomic diffusion along grain boundaries should be cut off in the remaining crystalline structure of substance; i.e., a clearly pronounced nanocrystalline structure must be prepared.

Figure 9 shows X-ray diffraction patterns for samples annealed at 900°C. According to the X-ray diffraction patterns, the recrystallization process is activated during annealing. The AlN and AlB_2 compounds were found to be the principal phases in the coating composition. Note that, according to theoretical data, the aluminum and titanium diborides are characterized by the same structure type and space group and have close lattice parameters (Table 3). Taking into account the initial phase composition of the sputtered cathode, we also exclude the presence of bivalent TiB_2 titanium boride in the coatings. The partial oxidation of the coating material (the presence of diffraction reflections of the α-Al_2O_3 phase) is due to the fact that the aluminum nitride decomposes at temperatures above 700°C, which forms an that is thermally stable at temperatures up to 1370°C [25].

The calculated lattice parameters of the phases in the coating are given in Table 3. It is shown that the lattice parameters of all phases agree well with tabulated data. This means that the conditions of condensation and subsequent annealing that we used allowed us to prepare a multiphase coating in which each phase has a continuous crystal lattice and does not form solid solutions with impurity atoms.

The size of crystallites L_{hkl} was estimated using broadening of diffraction reflections and relation [28]

$$L_{hkl} = \frac{\xi\lambda}{\beta\cos\theta}, \quad (2)$$

where L_{hkl} is the average size of crystallites along the normal to the reflecting surface; β is the physical broadening of reflection; λ = 2.2896 Å is the wavelength of X-ray radiation (Cr $K\alpha$); θ is the Bragg angle that corresponds to the reflection used for the calcula-

Table 3. Phase composition of the AlN–TiB_2–$TiSi_2$ coatings annealed at 900°C

Phase	Lattice, space group	Lattice parameters, Å				T_m, °C	Microhardness (H), GPa
		tabulated values		calculated values			
		a	c	a	c		
AlN	Hexagonal, $P6_3mc$ [26]	3.104 [26]	4.965 [26]	3.081	4.958	2400, decomposed [26]	–
TiB_2	Hexagonal, $P6/mmm$ [27]	3.0303 [27]	3.2295 [27]	3.038	3.227	2980 [27]	33 [27]
AlB_2	Hexagonal, $P6/mmm$[27]	3.0054 [27]	3.2528 [27]	3.010	3.225	1655 [27]	13.72 [27]
α-Al_2O_3	Rhombohedral, $R\bar{3}c$ [26]	4.7587 [25]	12.9929 [25]	4.745	12.845	2250 [25]	20 [25]

tions; and ξ is the factor that takes into account the indices of the reflecting plane. The range of ξ variations 0.98–1.39; for the calculations, we used $\xi = 1$.

Thus, annealing at 900°C leads to the crystallization of coating and the formation of nanocrystallites about 15 nm in size. The phase composition of the coating agrees adequately with data on the elemental composition of the coating. After annealing, the protective layer contains 38.07 at % B, 12.70 at % C, 8.32 at % N, 13.14 at % O, 18.30 at % Al, 2.70 at % Si, and 6.72 at % Ti. Carbon, the presence of which in the coating is determined by elemental analysis, does not form carbides in the coating. Therefore, we assume that carbon is present in the protective layer in the form of nanosized graphite inclusions, which make insignificant contributions to the X-ray diffraction pattern.

The phase composition of the coating across their depth was estimated qualitatively by small-angle X-ray scattering. The analysis of X-ray diffraction patterns taken at beam tilting angles of 3°, 10°, and 30° (Fig. 9) shows the following:

(1) The surface layer of the coating is saturated with aluminum (Al_2O_3) and titanium (β-TiO_2) oxide phases (Fig. 10, curve *1*), which, under normal conditions, can block the corrosion of material. However, the formation of oxide phases leads to an increase in the rough edges of the surface layers to 2 μm (Fig. 3a).

(2) As the distance from the coating surface increases (curves *2* and *3*), the concentration of boride phases increases, and the oxide component almost disappears. This must positively affect the adhesion of the coating on the substrate.

The coatings annealed at 1300°C consist of aluminum oxide and diboride crystallites 11–25 nm in size. The AlN compound was not found on the coating since AlN decomposes completely during annealing, and pure aluminum forms oxide. The α-Al_2O_3 film is formed on the surface and near the surface (Fig. 10, curves *2* and *3*); near the substrate, aluminum diboride AlB_2 dominates (Fig. 10, *1*). However, Ti and its compounds were not found in the coating. The X-ray diffraction data agree completely with data on the element composition of coatings (Table 2). We also assume that carbon is present in the coating in the form of small, slightly reflecting inclusions.

The irradiation of the surface of annealed samples with Au ions stimulates the further depletion of the surface of boron; this manifests in a relative decrease in the intensity of reflections of the aluminum boride (Fig. 10, curve *4*). The decrease in the roughness of the surface coating can also be classified as an ion-implantation effect, which manifests in a relatively low background spread of the diffraction pattern taken with sliding geometry.

The ability of materials to resist plastic deformation or brittle failure determines the field in which they can be applied. Therefore, to determine the optimum conditions of deposition and subsequent thermal annealing, mechanical tests, i.e., nanohardness tests and the determination of the modulus of elasticity (by procedure described in [29]), were performed. Figure 11 shows the dependence of the depth of nanoindenter penetration on the applied load. According to calculations, the nanohardness of the AlN–TiB_2–$TiSi_2$ coating in the initial state is 14.5 GPa, and the Young's modulus is 217 GPa. The behavior of the unloading

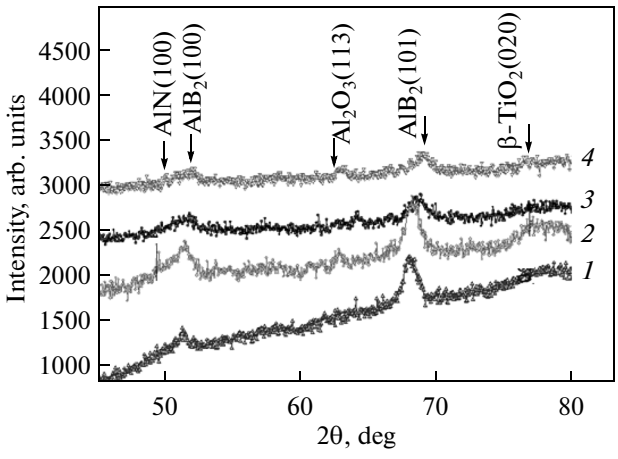

Fig. 10. Portions of X-ray diffraction patterns of the composite coating taken at tilting angles of (*1*) 30° (series 3), (*2*) 10° (series 3), (*3*) 3° (series 3), and (*4*) 2° (series 4).

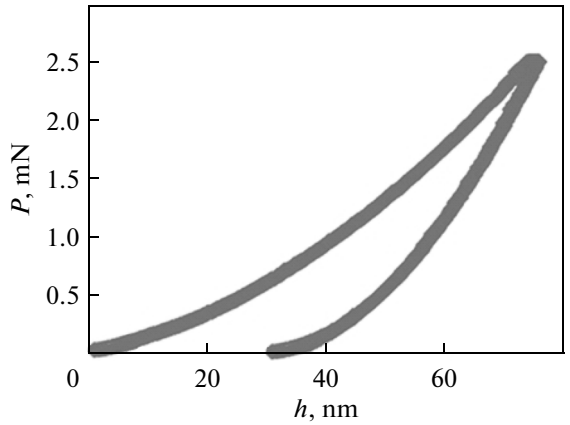

Fig. 11. Dependence of indentation depth h on the applied load P for the AlN–TiB_2–$TiSi_2$ coatings (series 1).

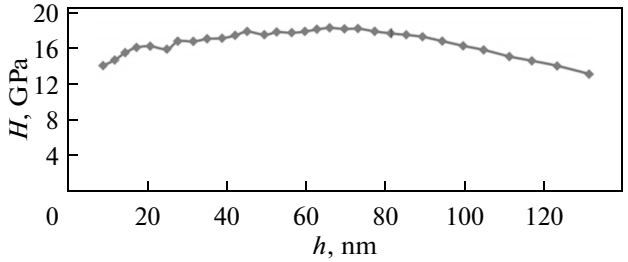

Fig. 12. Nanohardness distribution in depth of the protective coating.

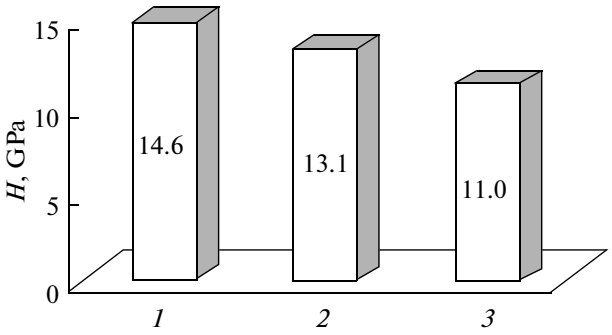

Fig. 13. Effect of annealing temperature on the nanohardness of AlN–TiB_2–$TiSi_2$ coatings: (*1*) series 1, initial state; (*2*) series 2, $T_{an} = 900°C$; and (*3*) series 3, $T_{an} = 1300°C$.

curve indicates that the material is characterized by adequate plasticity; i.e., during unloading, ~60% of the indentation depth is restored. The viscoplasticity index is ~0.7, which also characterizes the coating as an amorphous-like material.

The hardness distribution across the depth of protective coating was determined by dynamic nanoindentation. In this case, the 10-mN sinusoidal loading of the indenter was used. Figure 12 shows results of the tests. It was found that, at a distance of 40–80 nm from the surface, the hardness of the coating is about 17.5–18.5 GPa. Beginning from a depth of 85 nm, the hardness of the coating decreases; this results from the effect of the softer steel substrate. The high-temperature annealing of coatings leads to the decrease in the hardness of protective coating as compared to that of the initial state (Fig. 13). The reason for these changes is the structural and phase transformations of the material, which result in the partial restoration of the crystal structure from an amorphous-like structure and an increase in the crystallite size from 1 to 25 nm after annealing at 1300°C.

CONCLUSIONS

(1) The surface of a protective coating prepared by pulsed magnetron sputtering of the AlN–TiB_2–$TiSi_2$ target has a homogeneous structure characterized by rough microedges of no more than 1 μm in size.

(2) During the deposition of the material, an amorphous-like nanocrystalline structure is formed. The size of the ordering areas is about 1 nm.

(3) The magnetron sputtering of the material allows us to form a protective layer, the elemental composition of which is completely identical to that of sputtered targets. The annealing of samples at 900 and 1300°C leads to the formation of a base matrix that consists of Al, B, O and C atoms. Ti and Si atoms disappear from the protective layer composition.

(4) The annealing of samples at 1300°C activates the crystallization of the material, which results in the growth of the size of crystallites to 11–25 nm. The presence of oxygen in air leads to the saturation of the surface with α-Al_2O_3 and β-TiO_2 oxide phases and increase in the rough edge size to 2 μm. The composition of protective layer was found to include AlB_2 and TiB_2 boride phases, the contents of which increase in approaching the coating–substrate interface.

(5) The implantation of Au atoms into the ceramic coatings stimulates the diffusion of boron atoms toward the substrate and leads to a decrease in the surface roughness.

(6) The analysis of mechanical characteristics showed that, under the used deposition conditions, a coating is formed that is characterized by a nanohardness of 14.5 GPa and a modulus of elasticity of 217 GPa. The activation of crystallization processes at high temperatures allows us to obtain diffusion and a temperature-stable nanostructure. The hardness of the nanostructured coating is 25% lower than that of metastable coatings in the initial state.

ACKNOWLEDGMENTS

The work was carried out within the projects "Development of fundamentals of the formation of superhard nanostructured multicomponent coatings with high physico-mechanical properties" (grant no. 01124001382) and "Physical principles of plasma

tehnology for combined treatment of multicomponent materials and coatings" (grant no. 0113400137C).

REFERENCES

1. A. D. Pogrebnyak, A. P. Shpak, N. A. Azarenkov, and V. M. Beresnev, "Structures and properties of hard and superhard nanocomposite coatings," Phys.–Usp. **52**, 29–54 (2009).
2. B. U. Asanov and V. P. Makarov, "Nitride coatings obtained by vacuum-arc deposition," Vestn. Kyrg.-Ross. Slav. Univ., **2** (2), 11–23 (2002).
3. A. G. Molyar and A. I. Vasil'ev, "Effect of the regime of deposition of a titanium nitride coating on the process of its wear upon fretting corrosion." Trenie Iznos **13**, 350–355 (1992).
4. N. V. Dubovitskaya, L. D. Kolenchenko, and L. N. Larikov, "Structure and phase content of TiN coating on an austenitic steel," Izv. Akad. Nauk SSSR, Met., No. 3, 162–164 (1989).
5. P. I. Ignatenko, "Deposition of boride, nitride, and silicide coatings with desired crystal morphology and perfection," Tech. Phys. **56**, 264–268 (2011).
6. V. I. Bachurin, V. M. Vishnyakov, D. S. Kolligon, K. F. Minnebaev, V. E. Yurasova, "Hard coatings based on ternary compounds," Poverkhnost, No. 4, 106–110 (2005).
7. A. Venneman, H.-R. Stock, J. Kohlscheen, S. T. Rambad, and G. Erkens, "Oxidation resistance of titanium–aluminum–silicon nitride coatings," Surf. Coat. Technol. **174–175**, 408–415 (2003).
8. H. C. Barshilia, M. S. Prakash, A. Jain, and K. S. Rajam, "Structure, hardness and thermal stability of TiAlN and nanolayered TiAlN/CrN multilayer films," Vacuum **77**, 169–179 (2005).
9. A. D. Pogrebnjak and V. Beresnev, *Nanocoatings, Nanosystems, Nanotechnologies* (Bentham Sci., New York, 2012).
10. S. Veprek, M. G. J. Veprek-Heijman, P. Karvankova, and J. Prochazka, "Possible role of oxygen impurities in degradation of nc-TiN/a-Si_3N_4 nanocomposites," Thin Solid Films **23**, L17–L21 (2005).
11. A. D. Pogrebnjak, A. P. Shpak, V. M. Beresnev, M. V. Il'yashenko, F. F. Komarov, A. P. Shypylenko, M. V. Kaverin, P. V. Zukovski, Y. A. Kunitskyi, D. A. Kolesnikov, O. V. Kolisnichenko, and N. A. Makhmudov, "Structure and properties of nano- and microcomposite coating based on Ti–Si–N/WC–Co–Cr," Acta Phys. Polon. A **120**, 100–104 (2011).
12. V. I. Ivashchenko, S. Veprek, A. D. Pogrebnjak, and B. O. Postolnyi, "First-principles quantum molecular dynamics study of $Ti_xZr_{1-x}N_{(111)}/SiN_y$ heterostructures and comparison with experimental results," Sci. Technol. Adv. Mater. **15**, 025007 (2014).
13. A. D. Pogrebnjak, I. V. Yakushchenko, A. A. Bagdasaryan, O. V. Bondar, R. Krause-Rehberg, G. Abadias, P. Chartier, K. Oyoshi, Y. Takeda, V. M. Beresnev, and O. V. Sobol, "Microstructure, physical and chemical properties of nanostructured (Ti, Hf, Zr, V, Nb) N coatings under different deposition conditions," Mater. Chem. Phys. **147**, 1079–1091 (2014).
14. H. C. Barshilia, B. Deepthi, and K. S. Rajam, "Deposition and characterization of TiAlN/Si superhard nanocomposite coatings prepared by reactive direct current unbalanced magnetron sputtering," Vacuum **81**, 479–488 (2006).
15. N. A. Azarenkov, V. M. Beresnev, A. D. Pogrebnyak, and D. A. Kolesnikov, *Nanostruñtured Coatingd and Materials: Principles of Formation. Properties. Areas of Application, Peculiarities of Contemporary Nanostructured Direction in Nanotechnology* (LIBROKOM, Moscow, 2012) [in Russian].
16. H. Söderberg, M. Oden, J. M. Molina-Aldareguia, and L. Hultman, "Epitaxial stabilization of cubic-SiN_x in TiN/SiN_x multilayers," Appl. Phys. Lett. **97**, 114327 (2005).
17. K. Zhang, L. S. Wang, G. H. Yue, Y. Chen, D. L. Peng, Z. B. Qi, and Z. C. Wang, "Structure and mechanical properties of TiAlSiN/Si_3N_4 multilayer coatings," Surf. Coat. Technol. **205**, 3588–3595 (2011).
18. T. D. Nguyen, S. K. Kim, and D. B. Lee, "High-temperature oxidation of nano-multilayered TiAlCrSiN thin films in air," Surf. Coat. Technol. **204**, 697–704 (2009).
19. N. Fukumoto, H. Ezura, K. Yamamoto, A. Hotta, and T. Suzuki, "Effects of bilayer thickness and post-deposition annealing on the mechanical and structural properties of (Ti, Cr, Al)N/(Al, Si)N multilayer coatings," Surf. Coat. Technol. **203**, 1343–1348 (2009).
20. L. Ning, S. Veldhuis, and K. Yamamoto, "Investigation of wear behavior and chip formation for cutting tools with nano-multilayered TiAlCrN/NbN PVD coating," Int. J. Mach. Tool Manuf. **48**, 656–665 (2008).
21. R. Krause-Rehberg, A. D. Pogrebnyak, V. N. Borisyuk, M. V. Kaverin, A. G. Ponomarev, M. A. Bilokur, K. Oyoshi, Y. Takeda, V. M. Beresnev, and O. V. Sobol', "Analysis of local regions near interfaces in nanostructured multicomponent (Ti–Zr–Hf–V–Nb)N coatings produced by the cathodic-arc-vapor-deposition from an arc of an evaporating cathode," Phys. Met. Metallogr. **114**, 672–680 (2013).
22. V. M. Beresnev, I. N. Toryanik, O. V. Sobol', A. D. Pogrebnyak, A. Yu. Kropotov, N. G. Stervoedov, U. S. Nemchenko, D. A. Kolesnikov, S. A. Klimenko, and P. V. Turbin, "AlN–TiB_2–$TiSi_2$ coatings obtained by pulsed magnetron sputtering," Tech. Phys. **59**, 1220–1223 (2014).
23. A. M. Glezer, "Amorphous and nanocrystalline structures: Similarities, dissimilarities, and mutual transitions," Ros. Khim. Zh. **46** (5), 57–63 (2002).
24. N. A. Vatolin and E. A. Pastukhov, *Diffraction Studies of the Structure of High-Temperature Melts* (Nauka, Moscow, 1980) [in Russian].
25. A. L. Borisova, L. I. Adeeva, and V. N. Sladkova, "Phase transformations in gas-thermal coatings from aluminum oxide," Avtomat. Svarka, No. 9, 26–32 (1997).
26. G. V. Samsonov, *Nitrides* (Naukova Dumka, Kiev, 1969) [in Russian].
27. G. V. Samsonov, T. I. Serebryakova, and V. A. Neronov, *Borides* (Atomizdat, Moscow, 1975) [in Russian].
28. Ya. S. Umanskii, Yu. A. Skakov, A. N. Ivanov, and L. N. Rastorguev, *Crystallography, X-ray Diffraction, and Electron Microscopy* (Metallurgiya, Moscow, 1982) [in Russian].
29. A. D. Pogrebnjak, D. Eyidi, G. Abadias, O. V. Bondar, V. M. Beresnev, and O. V. Sobol, "Structure and properties of arc evaporated nanoscale TiN/MoN multilayered systems," Int. J. Refract. Metals Hard Mater. **48**, 222–228 (2015).

Translated by N. Kolchugina